UNIVERSITY OF CALIFORNIA,
IRVINE

Wideband Circularly Polarized Fabry–Pérot Cavity Antenna With Sparse Array

THESIS

submitted in partial satisfaction of the requirements
for the degree of

MASTER OF SCIENCE

in Electrical Engineering

by

Linjie Li

Thesis Committee:
Professor Filippo Capolino , Chair
Professor Franco De Flaviis
Assistant Professor Hamidreza Aghasi

2021

DEDICATION

To

my parents and friends

in recognition of their worth

and Prof. Capolino and Prof. Rebeiz

for their meticulous support

TABLE OF CONTENTS

LIST OF FIGURES

LIST OF TABLES

ACKNOWLEDGEMENTS

I would like to express my deepest appreciation to my committee chair, Professor Filippo Capolino, who has the attitude and the substance of a genius: he continually and convincingly conveyed an excitement in regard to teaching. Without his guidance and persistent help, this dissertation would not have been possible.

I would like to thank my committee members, Professor Franco De Flaviis and Professor Hamidreza Aghasi for their dedicated teaching in class EECS 182 and EECS 270E, which provide the essential background on future research.

I thank Prof. Rebeiz in University of California, San Diego for his approval to this work and the admission for his lab to work on microwave and phased- array.

ABSTRACT OF THE THESIS

Wideband Circularly Polarized Fabry–Pérot Cavity Antenna
With Sparse Array

by

Linjie Li

Master of Science in Electrical Engineering

University of California, Irvine, 2021

Professor Filippo Capolino , Chair

A Planar wideband, circularly polarized (CP) Fabry-Pérot cavity (FPC) antenna with a wideband CP excitation source is presented in this paper. The antenna is made of a finite size partially reflective surface (PRS) that because of its thickness exhibits a non-Foster response which results in wide gain bandwidth. Wideband patch antennas with sparse array located at the ground of an air-filled cavity is used to excite the cavity with a CP wave. The Thesis summarizes the final results of an investigation that lasted several months, where various feeding geometries generating CP were considered. Here, we report only the design that led to the best results during the investigation. Simulation results of the proposed FPC antenna indicate that such an antenna radiates a CP wave with high FBR where high antenna gain is achieved over wide relative impedance bandwidth of 13.7% around 22 GHz. The antenna radiates with a maximum gain of 17.5 dBic and -3 dB gain bandwidth of 10.4% with an axial ratio (AR) bandwidth of 7.9%.

INTRODUCTION

A. The overview of wideband Fabry–Pérot cavity (FPC) antennas design

Wideband Fabry–Pérot cavity (FPC) antennas received huge interest recently due to their simple, light-weight, and low profile structure as well as it provides a highly-efficient broadside narrow beam radiation over a wide gain bandwidth [1]–[9]. This 2-D class of leaky-wave antennas (LWAs) can serve as the potential candidate to be implemented in the new emerging broadband wireless communication technology where a high throughput data transfer is required. In general, the antenna structure formed by a grounded dialectic substrate with a partially reflective surface (PRS) mounted on top forming a cavity. The FPCs usually are excited by an electric source (patch) inside the cavity or by a magnetic source (slot) located on the ground plane [1], [10], [11] The operational frequency of these type of antennas mainly dictated by the FPC height (i.e., half-wavelength) and the PRS reflection phase.

It is well known that in the conventional FPC antenna design, the bandwidth-gain is relatively small. To solve this problem, two sets of methods are applied. The first is to optimize the feeds of the Fabry Perot Cavity. In [26]–[28], multilayers structure of the feed which stack-up patches is proposed, but the increasing is still not sufficient and the it increases the cost of PCB assembly. Other paper introduced the slot antenna as the feed which can obtain the 50% of return loss band ratio. However, because of its radiating principal, there is not perfect ground plane at the bottom layer so the back lobe is comparable to the main lobe which brings a lot of issues especially for the radar detection and satellite communications. Also, some other structure is designed to solve this bad front-back ratio. In [29], a metal box is located at the back of the feeds and it acts as the reflector in the whole structure so there is little field leaks to the back direction, but there are total 3 layers and 2 cavities and it needs a lot of bolts and screws to support them, which makes the design cumbersome and hard to build in the limited space.

The second set of the design focuses on the partially reflective surface design. In [8], the study of the numbers of the superstrate is proposed and it demonstrates that when more layers of superstrate are implemented, the higher gain is obtain but the bandwidth is also decreased and the product of gain- bandwidth does not been improved much. Because of the multi-superstrate, more resonance modes are inevitable. More important, it also increase the assembly difficulties. In [12], the new PRS design is proposed and it not only contains the dielectric superstrate but also a thin sheet of metal so there are more wave reflects in the cavity and so only one layer of partially reflective surface is required and do not need to build multilayers of partially reflective surface. However, it still does not make a big progress in increasing the bandwidth because the resonance condition of the cavity (Eqs. 6) is only satisfied in one frequency so it does not solve the problem in the principle level.

More recently, radiation properties from such FPC antenna formed by an electrically thick PRS, single or multiple stacks of thin metallic and/or dielectric layers, were studied which show an increase in the gain bandwidth of such antennas [2], [9]. Also, the methodology is well developed and in our design, the PRSs parameters of the thick PRS are optimized to exhibits locally a non-Foster response (a positive slope of the reflection phase versus frequency) when a plane wave imping at the bottom face of the PRS. With a proper choice of the cavity height, the antenna gain bandwidth is increased dramatically compared to FPCs forming by thin PRSs. Furthermore, transverse equivalate network (TEN) method can be adopted to analyze the antenna structure with the thick PRS where it is modeled as a two-port network in the TEN as shown in Fig. 1.

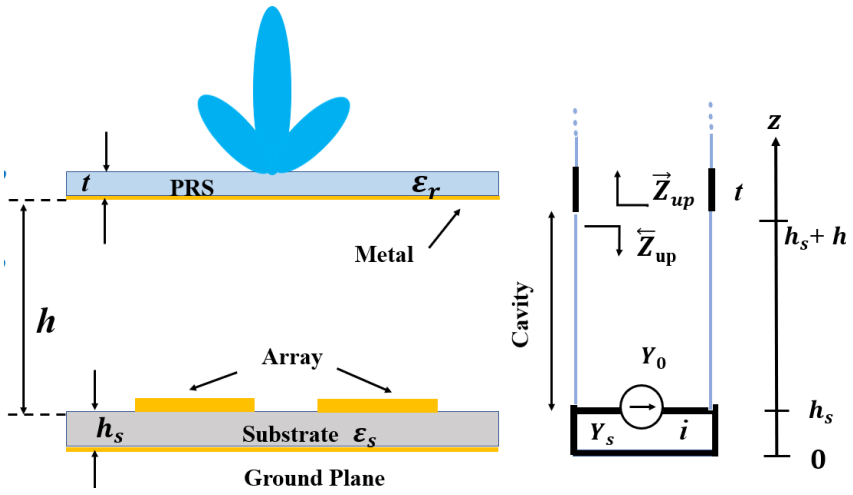

(a) (b)

Fig. 1. (a) Side view of the proposed antenna with a thick PRS and patch arrays. (b) Transverse equivalent network (TEN) for the proposed antenna with the thick PRS represented as a two-port network.

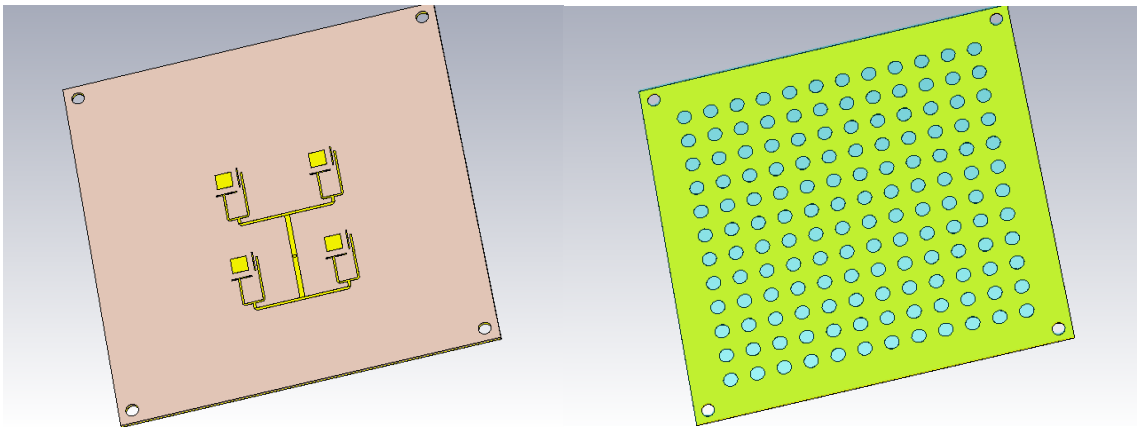

(a) (b)

Fig. 2. 3D view of the (a) patch antenna array (b) Partially reflective surface

B. The overview of circular polarized antennas design

Moreover, recent advance in the wireless technology demands the wireless communication system to be immune from the multipath interference in addition to the polarization mismatch between the transmitter and the receiver's antennas, so the wideband circular polarized antenna is quite needed and it also brings a lot of challenge to design the feed of FPC antenna. Two standard techniques which are used to generate CP wave is by implementing (i) a linear polarized (LP) primary source and the PRS supports the conversion to CP [18]–[22]., and (ii) a primary CP source i.e. circular waves bouncing inside the cavity [12]–[17].

For (i), to solve it in PRS design, a linear polarized (LP) primary source can be used and the PRS supports the conversion to CP [18]–[22].However, it decrease the gain of circular polarization and also the axial ratio bandwidth which is the key result for CP antenna is low. On the other hand, to achieve circular polarization in feed design , equal magnitude and 90° phase difference between two orthogonal radiation modes are required at the same time, and the required 90° phase difference is often generated in the following several ways.

A simple and conventional way is to split the two degenerate modes of a single-fed patch antenna by means of perturbation elements such as stubs, slots, or truncated elements [31]. When the two modes work below and above their respective resonant frequencies, they will lead and lag in phase, respectively, which results in phase difference [32]–[34]. For improvement, the method on stacked patches was developed to widen the axial-ratio (AR) bandwidth [35], [36].

Another straightforward method to produce 90° phase difference is to add a quarter wavelength delay line in the feeding network of dual-fed CP antennas [31], [37], [38]. Additional impedance-matching networks are usually required before the delay line to match two branches of the feeding line to the specified value of impedance at input port. Besides, a 3 dB coupler can alternatively produce 90° phase difference as well as equal magnitude. However, the coupler is designed by assuming that the load impedance is fixed as a constant value, which is contradictory to the frequency-dependent impedance of a patch radiator. Moreover, one port of the coupler has to be terminated by a resistor in order to absorb the unbalanced power [31], [39], [40]. For a transmitting antenna with high input

power, the power consumed resistor will raise a serious problem in power capacity.

At last, wideband 90° phase shifters [41]–[43] are utilized in the design of CP antenna, but the design of a phase shifter mainly concentrates on phase response, and magnitude cannot be taken into account simultaneously. Moreover, the phase shifter and radiator are designed separately and matched to the specified port impedance, such as 50 or 75 Ω, but the input impedance of a resonant patch radiator is highly frequency-dependent. Direct connection of a wideband phase shifter and a radiator will lead to a narrow AR bandwidth of circular polarization.

Recently, the concept of filtering antenna has been proposed and developed. In [44] and [45], two signal paths with coupled resonators are utilized to achieve wideband magnitude response of two orthogonal polarizations, and one extra resonator is added in one path to provide the 90° phase shift for CP radiation. In [46], codesign of three minima in the AR response of a CP patch antenna is tried by taking magnitude and phase into account simultaneously. In this thesis, we utilize this concept based on inherent phase properties of tapped-line and parallel coupled-line coupling structures and the details are in the Chapter 3.

C. Summary of the Introduction

Based on the above content, our design can achieve the wideband of return loss at K-band by implementing the well-designed feed and the thick PRS without the sacrifice of front to back ratio. More important, the structure is still compact and easy to assembly. For gain enhancement, we utilize the sparse array to increase the numbers of elements and the feeding line networks is still elegant.

In this thesis, in Chapter 1 we calculate the height of cavity by applying TL model , then in Chapter 2, the partially reflective surface (PRS) unit cell is proposed which has the Non-Foster behavior in desired band and predict the gain bandwidth by leaky wave analysis. In Chapter 3 , as the primary source of excitation, a wideband CP patch unit is designed to generate the circular polarization wave into the cavity. After that, a 2×2 sparse array is applied and it operates at K-band. Finally, we add the sparse array with the 14×14 PRS to form the completed Fabry Perot Cavity (FPC) Antenna and simulation results are in Chapter

4 . The proposed structure shows a 3 dB axial ratio (AR) bandwidth of 7.9% (20.6 – 22.3 GHz), a maximum gain of 17.5 dBic and gain bandwidth of 10.4% (19.8 – 22.1 GHz). Furthermore, the antenna exhibits an impedance bandwidth of 13.7% (20.4 – 23.4 GHz) which covers the entire -3 dB gain bandwidth.

CHAPTER 1 : THE DESIGN OF CAVITY HEIGHT

In [9]–[18], some theories have been rigorously carried out for cavities without the h_s-thick dielectric substrate. However, the presence of this dielectric substrate over the patched could not be ignored because it renders the cavity not only make up of air, so the leaky-wave analysis in [9]–[18] would be much complicated and cannot be completely implement in this design. Instead, the transmission line (TL) model in [10] is an effective tool for the patch as the feed to this cavity. Here we use that formalism and provide some design criteria and numerical calculations to show the Fabry Perot Cavity with the patch feed.

Firstly, the resonance condition (for real frequencies) is shown below.

$$Im\left(\vec{Z}_{up} + \overleftarrow{Z}_{up}\right) = 0 \qquad (1)$$

Note that $\vec{Z}_{up}$ is the impedance evaluated at $z = \lambda_0/2 - \Delta$ looking toward increasing z and. To determine the accurate cavity thickness , the small correction factor Δ is induced to indicate the effect of substrate in the cavity. We implement the input impedance formula in transmission line model in [2]. For $\overleftarrow{Z}_{up}$, we get

$$\overleftarrow{Z}_{up} = Z_0 \frac{jZ_S \tan(k_s\, h_s) + jZ_0 \tan(k_0\, h)}{Z_0 - Z_s \tan(k_s\, h_s) \tan(k_0\, h)} \qquad (2)$$

where the height of cavity h is

$$h = \lambda_0/2 - \Delta - h_s \qquad (3)$$

The k_s in Eqs. (2) is the wavenumber in the substrate with permittivity ε_s and k_0 is the wavenumber in free space. h_s is the substrate height and Z_0 , Z_S are the characteristics impedance in free space and in the substrate. For correction factor of the cavity thickness Δ, it is

$$\Delta = \frac{\lambda_0}{2\pi} \arctan\left[\frac{1}{\sqrt{\varepsilon_s}} \tan\left(\frac{2\pi}{\lambda_0} \sqrt{\varepsilon_s}\, h_s\right)\right] - h_s \qquad (4)$$

In our design, the substrate heights h_s is 0.762 mm, which is small enough compared to

the half wavelength at 21 GHz (7.14 mm), so the Δ in (3) can be approximated as (5)

$$\Delta \approx \frac{h_s^3}{3}\left(\frac{2\pi}{\lambda_0}\right)^2 (\varepsilon_s - 1) \qquad (5)$$

In our case, h_s= 0.762 mm, ε_s = 3.67 and λ_0 =14.29 mm (f_0 = 21 GHz), so the correction term becomes Δ = 0.08mm by calculating the Eqs . (5), therefore according to the Eqs . (3), the height of cavity h is 6.1 mm. If this value is chosen properly, the gain bandwidth would be broad and the simulation result would be shown in Chapter 4 to verify the above calculation.

CHAPTER 2 : THICK PARTIALLY REFLECTIVE SURFACE DESIGN AND LEAKY WAVE ANALYSIS

A. Thick PRS details

The partially reflective surface (PRS) is the main component in any FPC antenna that shapes the far-field angular and frequency power pattern [1]–[9]. A direct relation between the PRS reflection phase and frequency is obtained by the assumption of cavity resonance. By using a ray tracing model in [21], the ideal reflection phase for an FPC antenna is derived as

$$\varphi_{PRS}(\omega) = 2k_{z1}h + \pi(2n-1)\ , n = 1 \qquad (6)$$

The phase $\varphi_{PRS}(\omega)$ usually decreases with frequency, in accordance with Foster's theorem, while k_{z1} increase with frequency. It means that Eqs. (6) is only satisfied at one frequency for a given cavity height h.

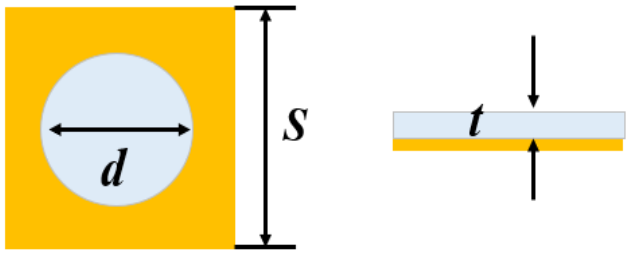

(a) (b)

Fig. 3. (a) (b) Top and side view of unit cell of the proposed PRS composes of a thin metallic sheet with holes of diameter D mounted on the bottom face of an electrically thick dielectric substrate with thickness t.

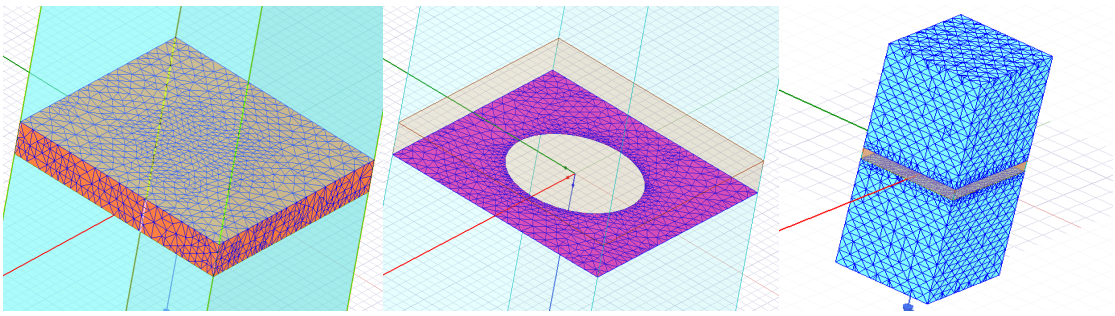

Fig. 4. Mesh Setting of PRS in HFSS

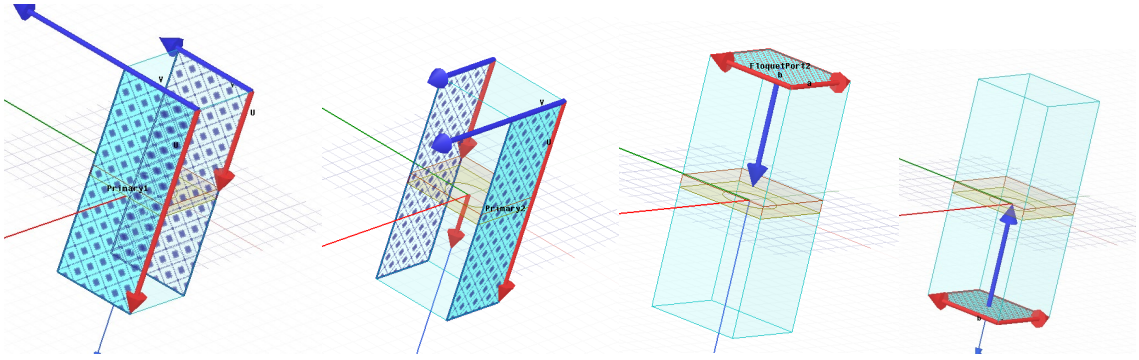

Fig. 5. Setting of Periodic Boundary Condition and Ports in HFSS

For the sake of wideband, it is desired to satisfy Eqs. (6) over the bandwidth of operation. If the phase $\varphi_{PRS}(\omega)$ experiences an increase in the frequency band but not the typical Foster-like frequency dependence (that has $\partial\varphi_{PRS}(\omega)/\partial\omega < 0$), the property of wideband can be achieved.

By following the design procedure discussed in [9], the PRS geometrical parameters are optimized to satisfy the FPC resonance condition at a wide frequency band. The PRS unit cell geometry is shown in Fig. 3. This structure consists of a thin metallic (copper) sheet with a 2-D infinite periodic (along x and y) circular holes with a diameter *d* etched at the bottom of a dielectric substrate of height t. Note that the dielectrics for the superstrate should be selected properly because there is a trade-off between the bandwidth and the gain enhancement. If we choose the dielectrics with lower permittivity, the band which meets the non- Foster behavior would be broad but there would be a little gain enhancement. In our case the patch is utilized as the feed for the cavity and it is well known that its bandwidth is around 5%, so this feed restricts the whole bandwidth at some extent. So we have chosen Rogers RT/duroid 6010.2LM with relative permittivity ε_r = 10.2 and a loss tangent of tan δ

= 0.0023 as the superstrate. The thickness of this superstrate is t = 0.635 mm and S = 5 mm ≈ 0.37 λ_0, where λ_0 is the operating free-space wavenumber at 22 GHz.

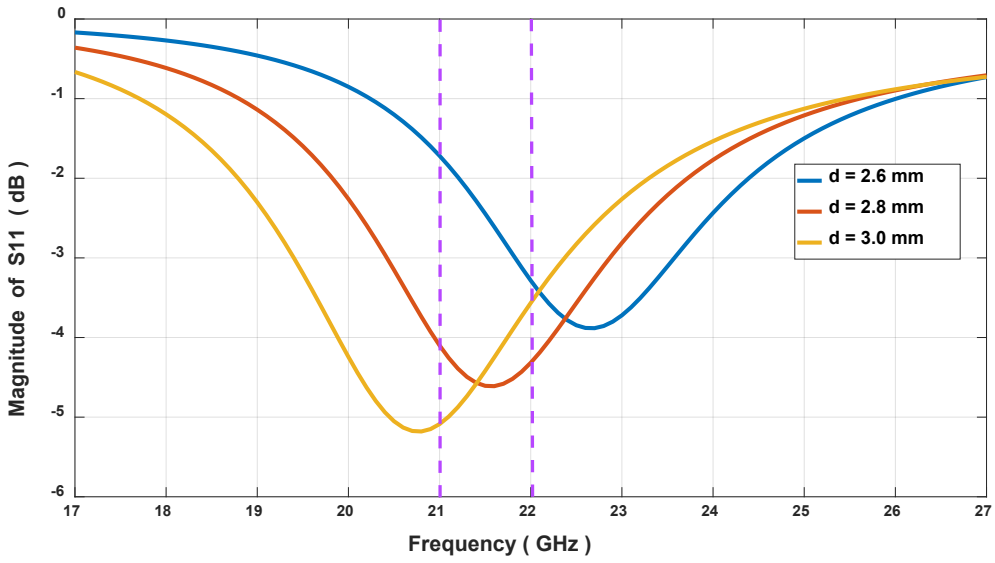

(a)

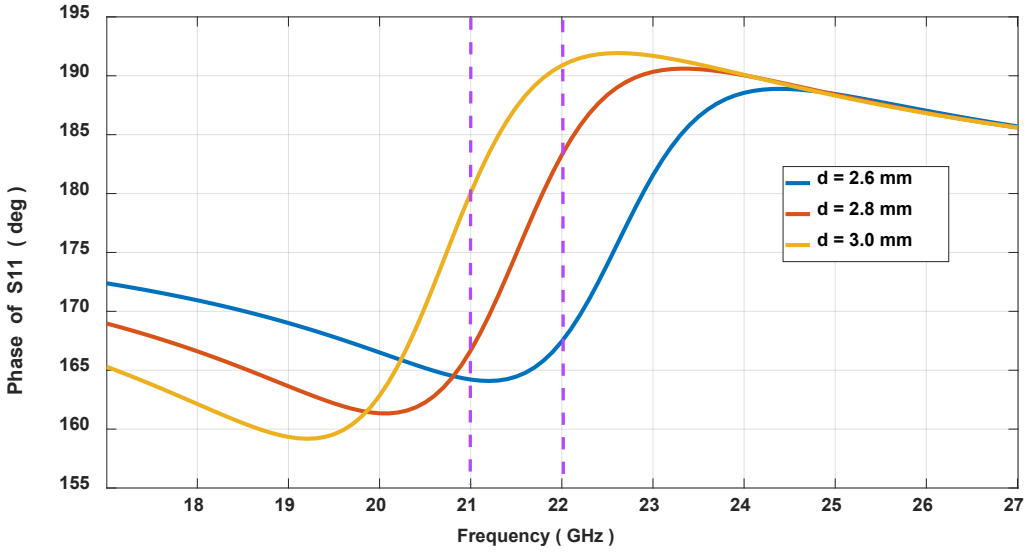

(b)

Fig. 6. (a)Magnitude and (b) phase of the reflection coefficient for the thick PRS with different diameter *d* of the hole on PRS formed by an infinite 2-D periodic unit cell. The dash line represents the desired band

For diameter *d* of the hole in PRS, it determines the center frequency of PRS and by varying the thick PRS geometrical parameters, a non-Foster behavior in a desired band could be obtained and a parameter study of diameter *d* is shown in Fig.6. The PRS unit cell is

simulated using Ansys HFSS with a periodic boundary condition when a plane wave impinging on the bottom face of the PRS as shown in Fig. 3(a). Note that as shown in Fig.5, the Floquet ports are redeemed to the top and bottom face of PRS to obtain the Y parameters. In Fig. 4, the fine enough mesh is set to increase the accuracy of the simulation result.

We can see that when d = 2.8 mm, the center frequency of the S11 is within the 21-22GHz desired band and also from 20 to 22 GHz, the Non-Foster behavior is obtained, and this is broad enough target a wideband FPC antenna with patch feed.

B. Leaky wave analysis by resonance condition

The FPC resonance condition is defined as the one that makes the imaginary part of the total admittance evaluated just below the FSS vanish.

$$Y_{tot}^{TE/TM}(k_t) = Y_{down}^{TE/TM} + Y_{up}^{TE/TM} = 0 \qquad (7)$$

where $k_t = \beta - i\alpha$, and β, α are LW propagation and attenuation constants, respectively. k_t also denotes the transverse complex wavenumber either along x or y which defined in Eqs. (7).

$$k_t = \sqrt{k_s^2 - k_{z,s}^2} \qquad (8)$$

$k_{z,s}$ is the longitude wavenumber and $k_s = 2\pi/\lambda_s$ is the wavenumber in different material. Note that in whole structure $k_{z,s}$ is different in air and substrate but the transverse complex wavenumber k_t remains same. The upward admittance $Y_{up}^{TE/TM}$ in Eqs. (6) is obtained by using simulation software HFSS to work out resonance equation (eqs.1) as

$$Y_{up} = Y_{11} - \frac{Y_{12} \cdot Y_{21}}{Y_0 + Y_{22}} \qquad (9)$$

where Y_{11}, Y_{12}, Y_{21} and Y_{22} are the elements of the Y-matrix related to the two-port admittance network model of the FSS that are calculated in HFSS relative to a single FSS unit cell.

Looking at the TL model, in Fig. 1 (b), the radiation area on bottom of the antenna, is modeled as a TL with length of with free-space characteristics impedance and a shorted TL

with the thickness of the dielectric slab (Rogers 4350B with dielectric constant ε_s, 3.56) of h_s = 0.762 mm (Eqs. 8)

$$Y_{down} = -j \cdot Y_0 \frac{Y_s - Y_0 \tan(k_{z0}\, h)\, \tan(k_{z1}\, h_s)}{Y_s \tan(k_{z0}\, h) + Y_0 \tan(k_{z1}\, h_s)} \qquad (10)$$

The characteristics admittance Y_s in the above equation is $Y_s^{TE} = k_{z1}/(\omega\mu_0\mu_r)$ or $Y_s^{TM} = (\omega\epsilon_0\epsilon_r)/\, k_{z0}$ for TE or TM mode, where ϵ_r and μ_r are the relative permittivity and permeability of the dielectric substrate, respectively. Similarly, Y_0 is the characteristics admittance in free space for TE or TM mode, $Y_0^{TE} = k_{z0}/(\omega\mu_0)$ or $Y_0^{TM} = (\omega\epsilon_0)/\, k_{z0}$.

Combining Eqs. (7) - (10), the unknown k_t could be calculated out and it contains the real and imaginary parts β, α , which demotes the propagation and attenuation constants for TE modes, and the normalized propagation (blue line) and attenuation constants (red line) are shown in Fig. 6 . The calculation is completed in software MATLAB 2020. Note that the maximum gain would appear when the propagation and attenuation constants are identical. According to the Fig. 7, it denotes that we obtain the maximum gain at the desired band.

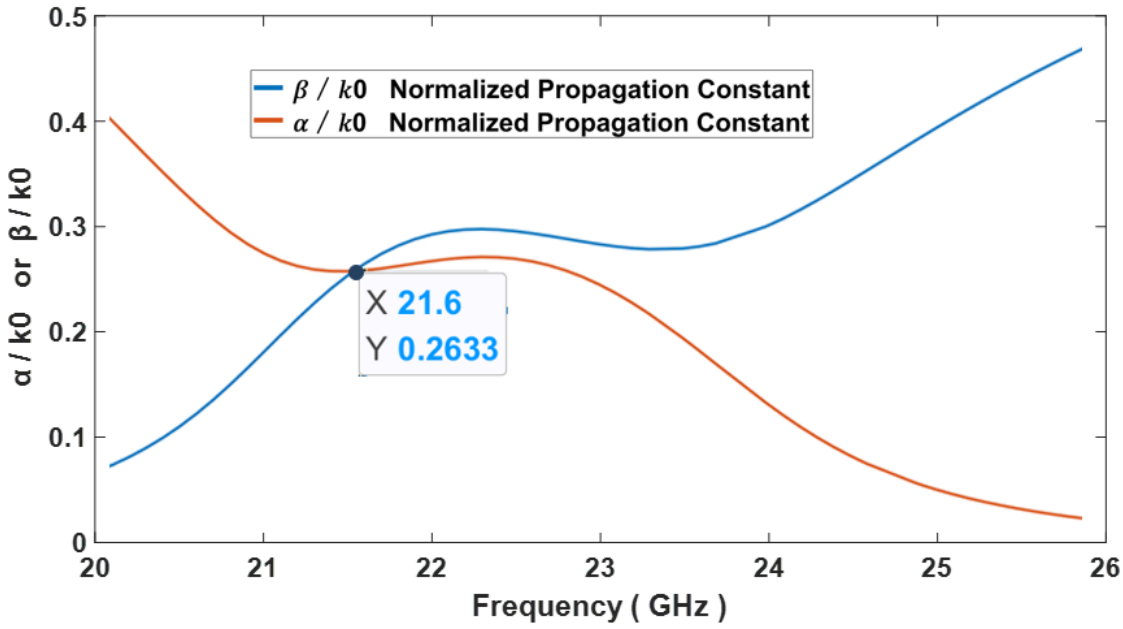

Fig. 7. TE Mode: Dispersion Diagram for the Normalized LW Phase and Attenuation Constants

CHAPTER 3 : SPARSE ARRAY AND CIRCULAR POLARIZED EXCITATION

For radiation elements, we have implemented a wideband CP patch antenna reported in [25] as a primary excitation with the tapped-line and coupled-line coupling structure. The geometry of the proposed antenna is demonstrated in Fig. 8. Two $\lambda/2$ resonators are utilized to excite the patch to obtain two orthogonal polarizations. After being tapped and coupled to the feeding line that provide the required 90° phase difference, an equal-magnitude T-junction is constructed to connect two ports.

The AR bandwidth of such elements is optimized varying the gap between resonators and patches in order to have an AR close to unity around 21.5 GHz. The design details is listed in Table.1 .

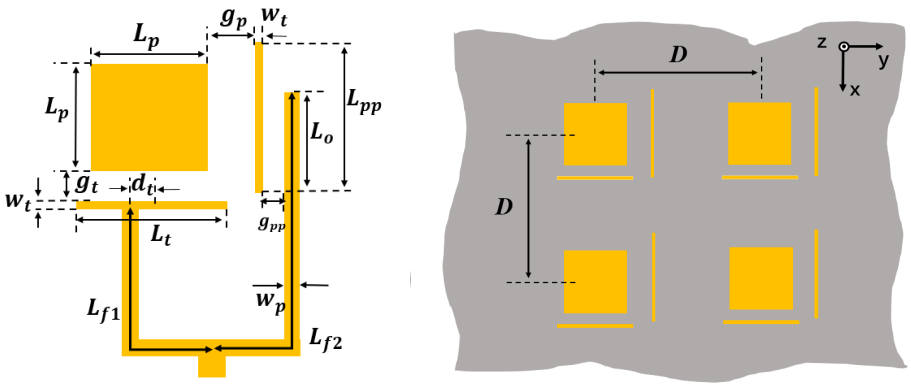

(a) (b)

Fig. 8. (a) The geometry details of circular polarization patch element
(b) Array configuration with spacing D

TABLE 1

Design Parameters for The Structure in Fig. 7

Para.	Value (mm)	Para.	Value (mm)	Para.	Value (mm)
L_{pp}	3.86	L_o	2.80	g_t	1.20
L_p	2.95	L_t	3.80	w_p	0.35
L_{f1}	7.27	g_p	1.05	w_t	0.20
L_{f2}	10.90	g_{pp}	0.40	d_t	0.50

In our design as shown in Fig.8 (a) , one patch has two $\lambda/2$ resonators at two edges to excite two orthogonal polarizations and it leads that one single element occupy much more areas than the traditional circular polarization patch design. In addition, more feeding lines are utilized so the coupling among them should also be considered. These bring a large challenge to design the feeding networks and determine the whole array configuration.

As discussed in [10], using a superstrate layer above the radiated elements can keep a reasonably large bandwidth and also increase the directivity by having an array of a few radiating elements, which spacing is larger than one wavelength. In addition, in this method the coupling between elements is also mitigated and sidelobe level (SLL) still maintain a reasonable value, so the sparse array is used to alleviate the coupling between elements which degrade axial ratio significantly. However, according to the array theory, when the spacing is increasing, the side lobe would be higher and at some points, it even can be comparable to the main lobe, so the study of the side lobe level is significant for the sparse array.

The side lobe levels in different spacing is listed in Table.2. Note that the side lobe level here is the ratio between first side lobe and the main lobe and the simulation is done in software CST Studio Suite 2018. The spacing $D = 17$ mm $= 1.25\ \lambda_0$ is chosen as its relatively low side lobe levels and the enough space for lines arrangements.

TABLE 2

Side Lobes Level of FPC Antenna (14 ×14 unit PRS) with Bolts for Different Spacing D between Elements

	Freq = 21 GHz		Freq = 22 GHz	
Spacing D	xz-plane	yz-plane	xz- plane	yz-plane
13 mm	-12.5 dB	-13.6 dB	-8.3 dB	-12.2 dB
15 mm	-9.0 dB	-6.6 dB	-5.3 dB	-3.0 dB
16 mm	-7.1 dB	-6.3 dB	-6.2 dB	-4.2 dB
17 mm	-7.6 dB	-7.7 dB	-6.7 dB	-7.1 dB
18 mm	-3.0 dB	-5.6 dB	-5.1 dB	-6.7 dB
19 mm	-4.8 dB	-6.6 dB	-5.2 dB	-6.0 dB
21 mm	-8.5 dB	-9.0 dB	-7.3 dB	-5.3 dB

CHAPTER 4 : FULL – WAVE SIMULATION RESULT FOR WIDEBAND CP FPC ANTENNA

In PRS, there should be enough numbers of unit cells shown in Fig. 3, because analysis in the above chapters is done when assume the PRS has the infinite number of unit cells and also the boundary condition of simulation in HFSS is periodic condition which denotes the infinite number of unit cell. In addition, it is impossible to build a infinite PRS in practice so the PRS needs should have enough number of unit cells but its area should be acceptable. We build three whole FPC antenna with different numbers: 12×12, 14×14 and 16×16 unit cells. To ensure the accuracy of the simulation, the finer meshes are applied to patches and the PRS on the superstrate, as shown in Fig.9

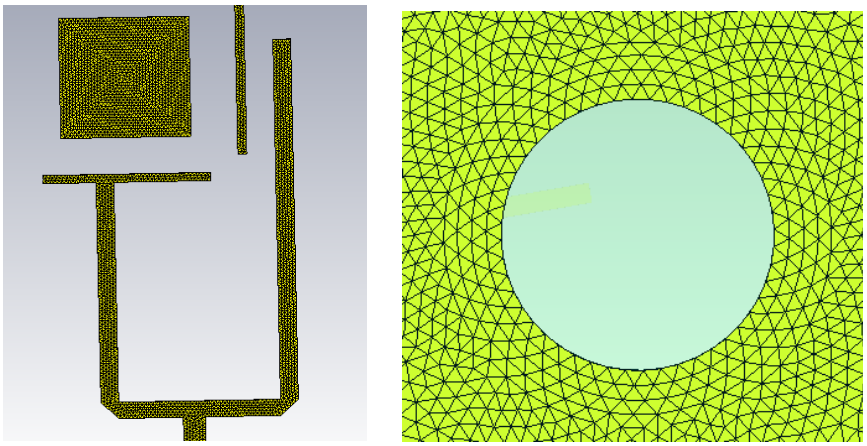

(a) (b)

Fig. 9. The meshes setting of (a) the patch (b) PRS on the superstrate

The S11 and realized gain results versus frequency are plotted in Fig.10. The simulation is completed in CST Studio Suite 2018. Note that the realized gain is generally smaller than the gain as it takes into account the impedance mismatch loss and the formula is $Gain_{realized} = 4\pi \times P_{radiated\ per\ unit\ solid\ angle}/P_{Stimulated}$.

In these three cases, the band that S11 lower than -10dB is 20.4 - 23.4 GHz (13.7%) , while the frequency ratio of the traditional patch is only around 5 %, which denotes a frequency enhancement. For gain curves, a maximum gain of 17.5 dB and a -3 dB gain bandwidth of 19.8 - 22.1 GHz (10. 4%) are obtained, while a 2× 2 patch array only has the

gain around 11 dB. The curves in Fig.10 also indicates that larger PRS obtains higher gain and it can be explained by the formula $Directivity = A_{eff} \times 4\pi/\lambda^2$, where A_{eff} is the effective aperture of the antenna and the lager PRS has larger aperture. We can also find that there are little differences between the gain curves of 14×14 and 16×16 unit cells. This is because at these points the PRS are large enough and the E-field at the edge is low enough so the increase of A_{eff} is subtle. After considering the cost and area, the 14×14 PRS meets the design requirement best in these cases.

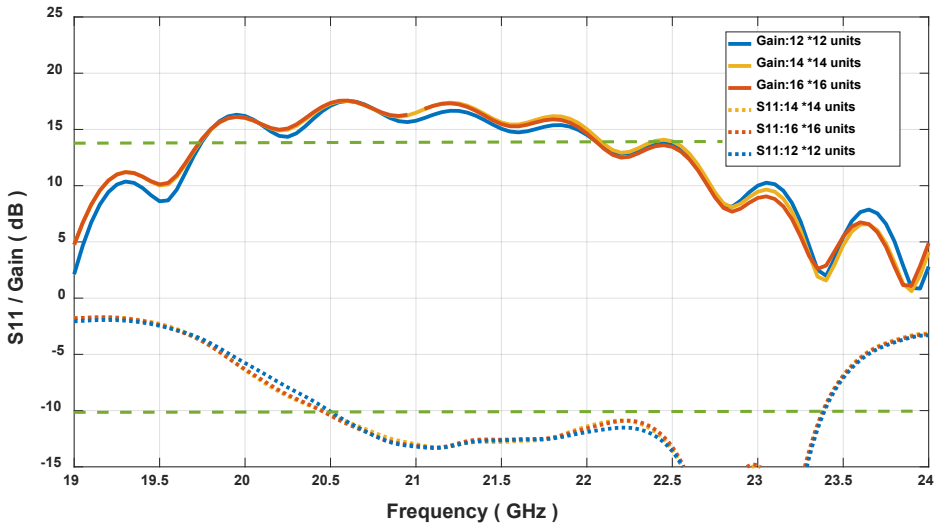

Fig. 10 . The S11 versus frequency result (red line) and the broadside realized gain of LHCP versus frequency with different numbers of unit cells on PRS

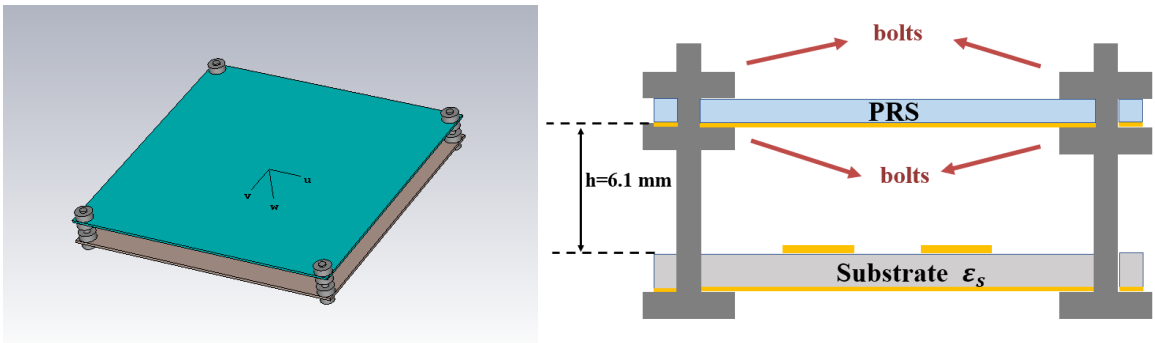

(a) (b)

Fig. 11. (a) The 3D view (b) The transverse view of the whole antenna with bolts

As shown in Fig. 11, to support the PRS, plastic bolts and screws are assembled at the edge of the structure in the software CST Studio Suite 2018 and these bolts and screws might worsen the AR bandwidth and deform the radiation pattern, so the study of the E - field distribution is necessary. We designed a finite FPC antenna with thick PRS using 14 × 14 unit cells on top of an cavity of height h = 6.1 mm with overall antenna dimensions of 80 mm × 80 mm in CST Studio Suite 2018. The primary feed of the cavity is the proposed 2×2 sparse patch array.

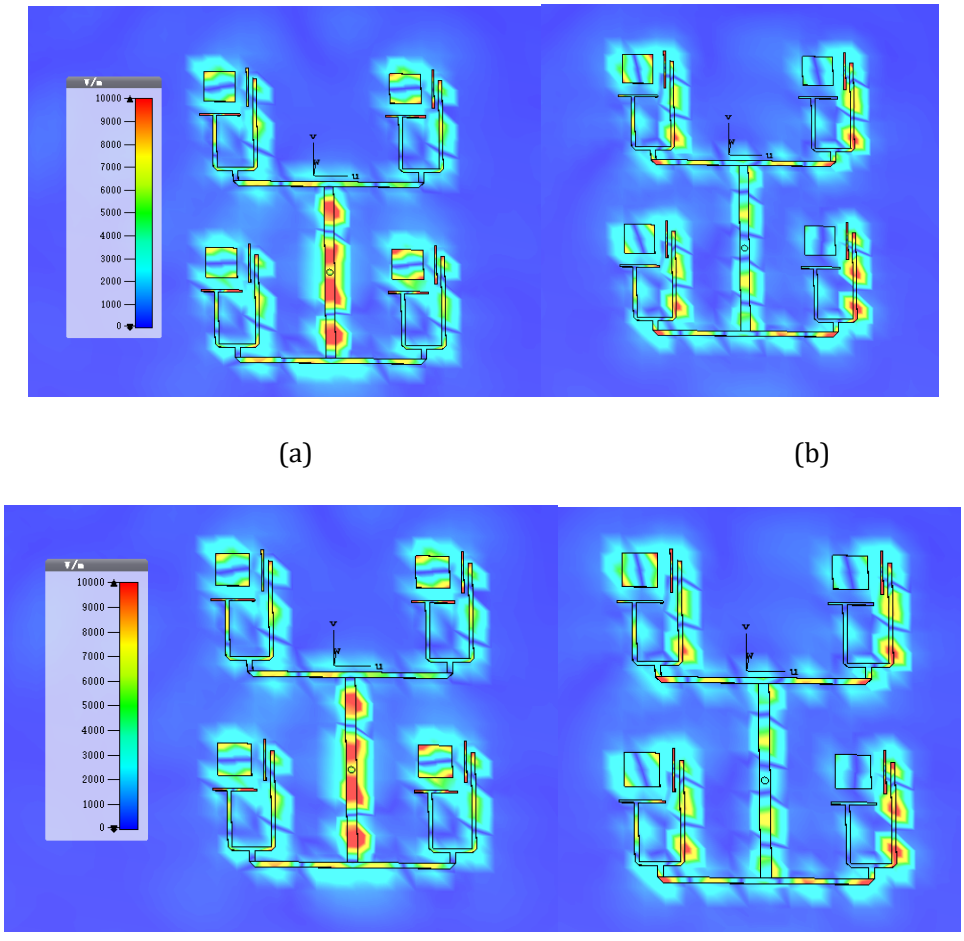

(a) (b)

(c) (d)

Fig. 12. Simulation results of E-field magnitude distributions of the upper surface of CP patch antennas at 21.5 GHz with different time t in one period T (a) $t = 0$. (b) $t = 1/4\ T$. (c) $t = 2/4\ T$. (d) $t = 3/4\ T$.

Fig. 12. shows that in the whole period T, the map of E -field of patches changes 90° at each quarter of the period T and it denotes that this patch sparse array provides the circular polarization wave to the cavity. Also, the E- field magnitude of the middle line of upper

surface of substrate in yz-plane direction at the edge is plotted in Fig. 13 and it shows that the intensity at the edge is much low. It also predicts that the substrate is large enough to mitigate the edge effect and surface wave reflection. Note that 14×14 PRS is implemented and there is two 5 mm-extra space for bolts assembly.

To evaluate the circular polarization performance, the axial ratio which defined as the ratio between the major and minor axis of a circularly polarized antenna pattern is introduced. This ratio tells us the deviation of an antenna from the ideal case of circular polarization over a specified angular range. In general the AR (axial ratio) bandwidth is the band which AR is below the -3 dB. The axial ratio result in Fig.14 denotes the 3dB axial ratio bandwidth does not change much and in this work with bolts, it is 20.6 -22.3 GHz (7.9%) , whereas in traditional circular polarization antenna design, it is only around 5%.

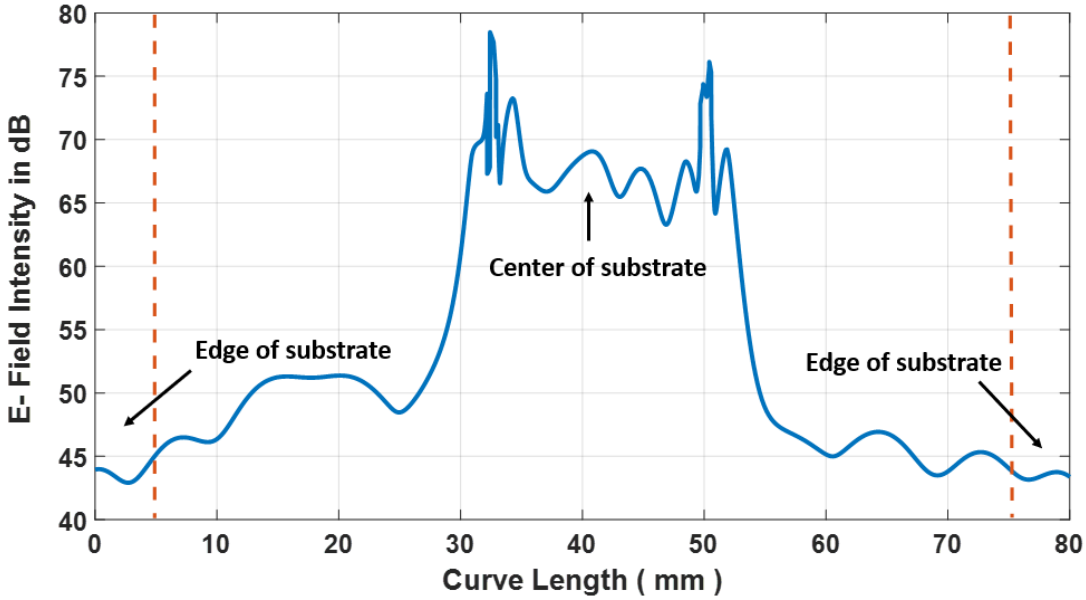

Fig. 13 The E-field magnitude of the middle line of upper surface of substrate when scanning y-direction (Fig.8 show) .14×14 PRS is used and the areas between dash line and y axis are for bolts space

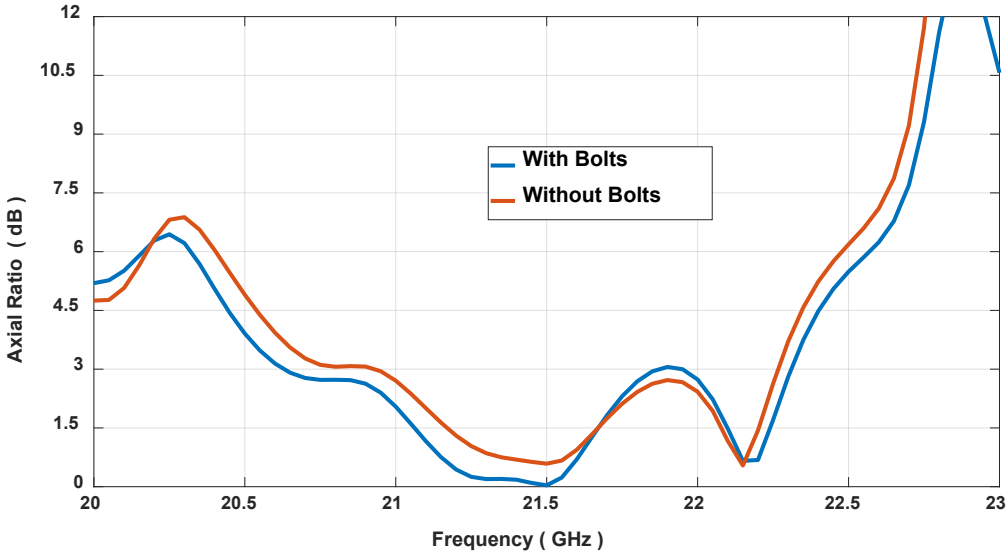

Fig. 14 . The axial ratio versus frequency result of proposed FPC antenna (14×14 PRS) with and without bolts

Furthermore, the simulated radiation efficiency (defined as the ratio of gain to directivity or equally the ratio between the radiated power to the accepted power of the antenna: the radiated power in all directions over the accepted power, $e_{rad} = Gain\ (\theta, \phi)/\ Directivity\ (\theta, \phi) = P_{rad}/P_{acc}$) is calculated in software CST Studio Suite 2018, and the result shows that it is above 85% over the entire antenna operational frequency band.

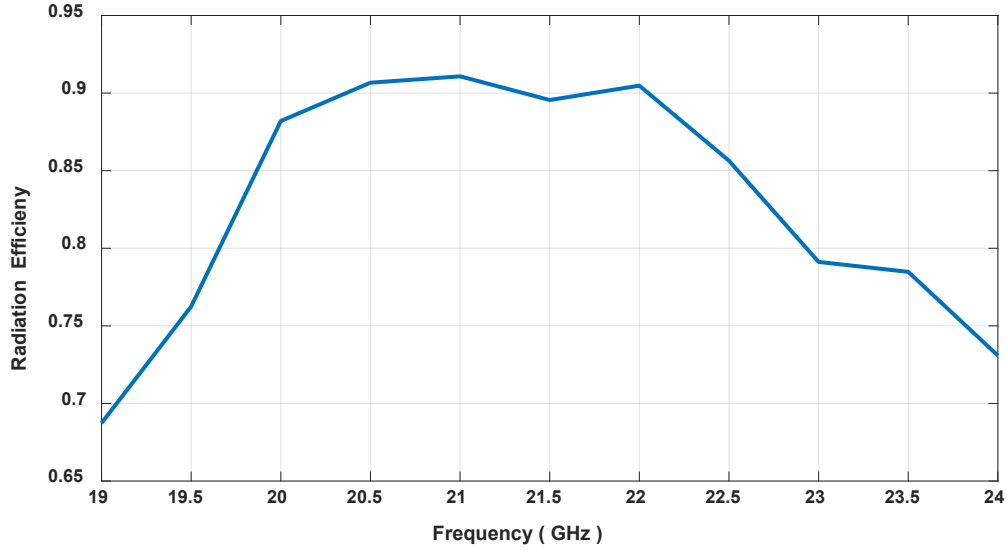

Fig. 15. The radiation efficiency versus frequency result of proposed FPC antenna (14×14 PRS) with bolts

In Fig. 16, the E – Field intensity distribution of PRS shows that the PRS unit at the center of the array has much higher E- field intensity than the PRS unit at the edge. It denotes that the main beam radiates at the broadside and the superstrate is large enough.

A gain pattern of the simulated antenna at 21 GHz and 22 GHz for xz-plane and yz-plane shown in Figs. 17 and 18 respectively. The patterns show the proposed antenna radiates at broadside and still maintains a low side lobe level although the spacing between elements is 1.25 λ_0 . Additionally, the back lobe also is -25 dB lower than the main beam, which can be explained by the existence of ground plane in the bottom layer of substrate. The results show that the proposed the whole antenna work well at K- band and it can also contain more patches and be extended to larger array to get higher gain.

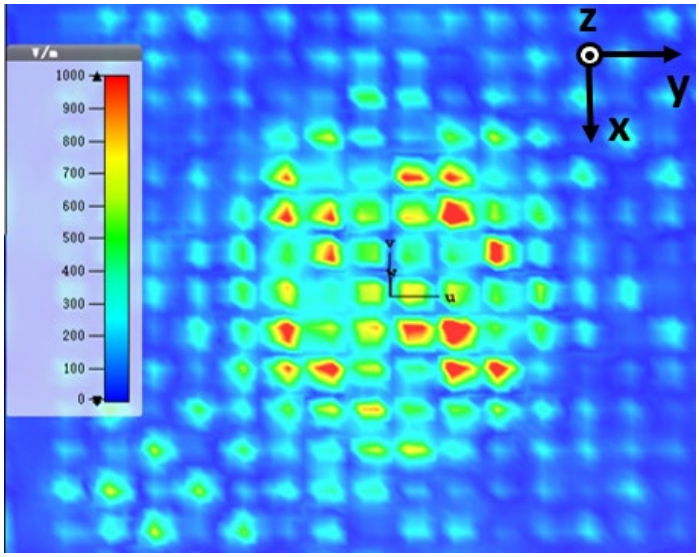

Fig. 16 . Simulated E- Field magnitude map of the upper surface of superstrate in PRS at 21.5 GHz

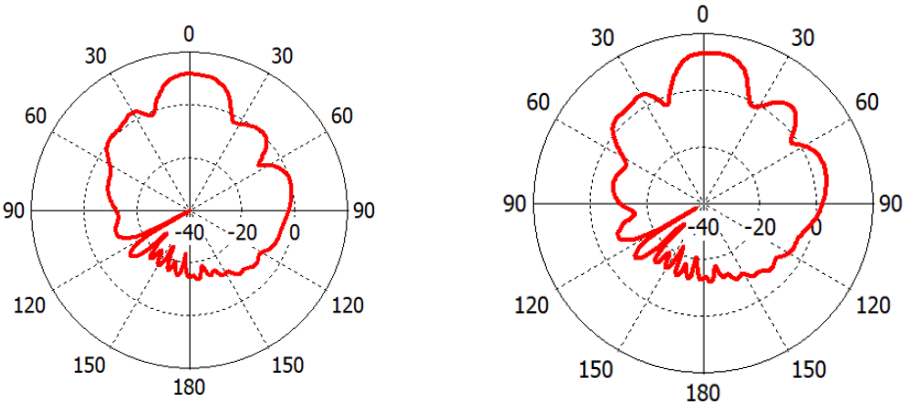

Fig. 17. Simulated gain pattern for xz - plane for LHCP at (a) 21 GHz and (b)22 GHz

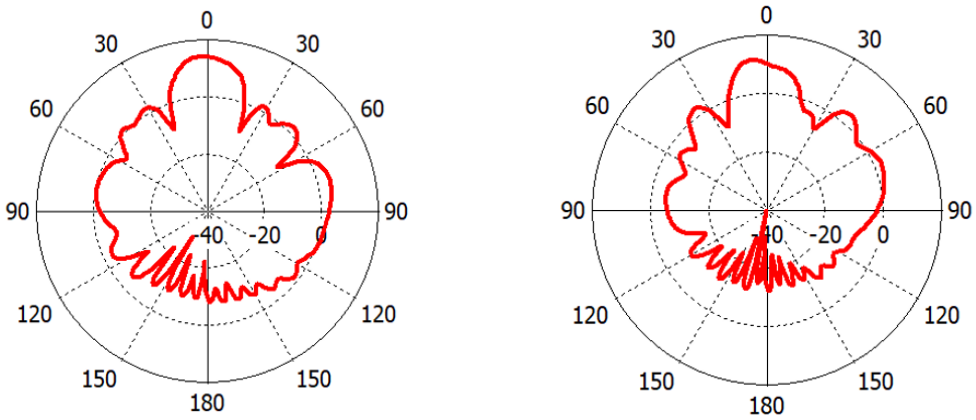

(a) (b)

Fig. 18. Simulated gain pattern for yz- plane for LHCP at (a) 21 GHz and (b)22 GHz

CONCLUSION

Firstly, we designed an optimized Fabry Perot Cavity including the height which determines the resonance frequency and the thick, partially reflective surface unit cell which obtain the non- Foster behavior in the wideband. Secondly, the wideband CP patch antenna is proposed to act as the excitation source to the whole structure. Finally, we properly arrange the patches in sparse array which increases the gain and obtain a -7 dB side lobe level.

The truncated structure possesses a wide -3 dB gain bandwidth of (19.8 - 22.1 GHz with a ratio of 10.4%), an axial ratio bandwidth of (20.6 -22.3 GHz with a ratio of 7.9%) , a wide S11 -10dB band with 20.4 - 23.4 GHz (13.7%) and a maximum broadside gain of 17.5 dBic, which shows a gain enhancement compared with normal patch arrays . The proposed wideband CP antenna gives a potential to be widely used in a satellite application in addition to a multipath interference environment.

REFERENCE

[1] G. V. Trentini, "Partially reflecting sheet arrays," IRE Trans. Antennas Propag., vol. 4, no. 4, pp. 666–671, Oct. 1956.

[2] A. P. Feresidis and J. C. Vardaxoglou, "High gain planar antenna using optimised partially reflective surfaces," IEE Proc.-Microw. Antennas Propag., vol. 148, no. 6, pp. 345–350, 2001.

[3] G. Lovat, P. Burghignoli, and D. R. Jackson, "Fundamental properties and optimization of broadside radiation from uniform leaky-wave antennas," IEEE Trans. Antennas Propag., vol. 54, no. 5, pp. 1442–1452, May 2006.

[4] G. Lovat, P. Burghignoli, F. Capolino, and D. R. Jackson, "Highly-directive planar leaky-wave antennas: a comparison between metamaterial-based and conventional designs," Proc. Eur. Microw. Assoc. Vol, vol. 12, p. 21, 2006.

[5] A. Hosseini, A. T. Almutawa, F. Capolino, and D. R. Jackson, "V-band wideband Fabry-Pérot cavity antenna made of thick partially-reflective surface," in 2016 IEEE International Symposium on Antennas and Propagation (APSURSI), 2016, pp. 349–350.

[6] A. Hosseini, F. De Flaviis, and F. Capolino, "Design formulas for planar Fabry–Pérot cavity antennas formed by thick partially reflective surfaces," IEEE Trans. Antennas Propag., vol. 64, no. 12, pp. 5487–5491, Dec. 2016.

[7] A. Hosseini, A. T. Almutawa, F. Capolino, and D. R. Jackson, "Wideband single-layer Fabry-Pérot cavity antenna with a radial variation of the cavity permittivity," in 2017 IEEE International Symposium on Antennas and Propagation USNC/URSI National Radio Science Meeting, 2017, pp. 2659–2660.

[8] S. Sengupta, D. R. Jackson, A. T. Almutawa, H. Kazemi, F. Capolino, and S. A. Long, "Radiation properties of a 2-D periodic leaky-wave antenna," IEEE Trans. Antennas Propag., vol. 67, no. 6, pp. 3560–3573, Jun. 2019.

[9] A. T. Almutawa, A. Hosseini, D. R. Jackson, and F. Capolino, "Leaky-wave analysis of wideband planar Fabry-Pérot cavity antennas formed by a thick PRS," IEEE Trans. Antennas Propag., 2019.

[10] R. Gardelli, M. Albani, and F. Capolino, "Array thinning by using antennas in a Fabry–Perot cavity for gain enhancement," IEEE Trans. Antennas Propag., vol. 54, no. 7, pp. 1979–1990, Jul. 2006.

[11] D. R. Jackson et al., "The fundamental physics of directive beaming at microwave and optical frequencies and the role of leaky waves," Proc. IEEE, vol. 99, no. 10, pp. 1780–1805, 2011.

[12] B. Ratni, A. de Lustrac, S. Villers, and S. N. Burokur, "Low-profile circularly polarized fabry–perot cavity antenna," Microw. Opt. Technol. Lett., vol. 58, no. 12, pp. 2957–2960, 2016.

[13] H. H. Tran and I. Park, "Compact wideband circularly polarised resonant cavity antenna using a single dielectric superstrate," Antennas Propag. IET Microw., vol. 10, no. 7, pp. 729–736, 2016.

[14] Z. Liu and W. Lu, "Low-profile design of broadband high gain circularly polarized Fabry-Perot resonator antenna and its array with linearly polarized feed," IEEE Access, vol. 5, pp. 7164–7172, 2017.

[15] Z.-G. Liu and W.-B. Lu, "Broadband design of circularly polarized high-gain Fabry-Perot resonator antenna with simple array thinning technique," Microw. Opt. Technol. Lett., vol. 59, no. 12, pp. 3171–3176, 2017.

[16] S. Kabiri, E. Kornaros, and F. De Flaviis, "Wideband circular polarized Fabry-Perot cavity antennas for V-band indoor point-to-point communications," Electromagnetics, vol. 39, no. 3, pp. 198–216, Apr. 2019.

[17] W. Cao, X. Lv, Q. Wang, Y. Zhao, and X. Yang, "Wideband circularly polarized Fabry–Perot resonator antenna in Ku-band," IEEE Antennas Wirel. Propag. Lett., vol. 18, no. 4, pp. 586–590, Apr. 2019.

[18] S. A. Muhammad, R. Sauleau, L. Le Coq, and H. Legay, "Self-generation of circular polarization using compact Fabry–Perot cavity antennas," IEEE Antennas Wirel. Propag. Lett., vol. 10, pp. 907–910, 2011.

[19] R. Orr, G. Goussetis, and V. Fusco, "Design method for circularly polarized Fabry–Perot cavity antennas," IEEE Trans. Antennas Propag., vol. 62, no. 1, pp. 19–26, Jan. 2014.

[20] Z. Liu, Z. Cao, and L. Wu, "Compact low-profile circularly polarized Fabry–Perot resonator antenna fed by linearly polarized microstrip patch," IEEE Antennas Wirel. Propag. Lett., vol. 15, pp. 524–527, 2016.

[21] M. Akbari, S. Gupta, M. Farahani, A. R. Sebak, and T. A. Denidni, "Gain enhancement of circularly polarized dielectric resonator antenna based on FSS superstrate for MMW applications," IEEE Trans. Antennas Propag., vol. 64, no. 12, pp. 5542–5546, Dec. 2016.

[22] A. Calleau, M. García-Vigueras, H. Legay, R. Sauleau, and M. Ettorre, "Circularly Polarized Fabry–Perot Antenna Using a Hybrid Leaky-Wave Mode," IEEE Trans. Antennas Propag., vol. 67, no. 9, pp. 5867–5876, Sep. 2019.

[23] Y.-X. Zhang, Y.-C. Jiao, H. Zhang, and Y. Gao, "A simple broadband flat-gain circularly polarized aperture antenna with multiple radiation modes," Prog. Electromagn. Res. C, vol. 81, pp. 1–10, 2018.

[24] V. R. Komanduri, D. R. Jackson, and S. A. Long, "Radiation characteristics of finite-length 1D-uniform leaky wave antennas radiating at broadside," in 2010 IEEE Antennas and Propagation Society International Symposium, 2010, pp. 1–4.

[25] Qiong-Sen Wu , Xiao Zhang , and Lei Zhu, "A Feeding Technique for Wideband CP Patch Antenna Based on 90° Phase Difference Between Tapped Line and Parallel Coupled Line," IEEE Trans. Antennas Propag., vol. 18, no. 7, pp. 1468–1471, July 2019.

[26] S. Sierra-Garcia and J. Laurin, "Study of a CPW inductively coupled slot antenna," IEEE Trans. Antennas Propag., vol. 47, no. 1, pp. 58 – 64, Jan. 1999.

[27] Q. Meide, M. Simcoe, and G. V. Eleftheriades, "Radiation efficiency of printed slot antennas backed by a ground reflector," presented at the IEEE Int. Symp. Antennas Propag., Salt Lake City, UT, USA, Jul. 2000.

[28] M. Ettorre, S. Bruni, G. Gerini, A. Neto, N. Llombart, and S. Maci, "Sector PCS-EBG antenna for low-cost high-directivity applications," IEEE Antennas Wirel. Propag. Lett., vol. 6, pp. 537 – 539, Nov. 2007.

[29] F. Ohnimus, I. Ndip, S. Guttowski, and H. Reichl, "An efficient and broadband slot antenna for 60 GHz wireless applications," in Proc. Electrical Design of Advanced Packaging and Systems Symp., Seoul, Dec. 2008, pp. 69 – 72.

[30] S. K. Podilchak, A. P. Freundorfer, and Y. M. M. Antar, "A planar cavity based antenna by leaky parallel-plate wave guiding and practical surface-wave launching," in Proc. IEEE Int. Symp. Antennas Propag., Toronto, ON, Jul. 2010, pp. 1 – 4.

[31] M. Haneishi and Y. Suzuki, "Circular polarization and bandwidth," in Handbook of Microstrip Antennas. London, U.K.: Peregrinus, 1989,pp. 220–273.

[32] S.D. Targonski andD.M. Pozar, "Design of wideband circularly polarized aperture-coupled microstrip

antennas," IEEE Trans. Antennas Propag., vol. 41, no. 2, pp. 214–220, Feb. 1993.

[33] K.-F. Tong and T.-P. Wong, "Circularly polarized U-slot antenna," IEEE Trans. Antennas Propag., vol. 55, no. 8, pp. 2382–2385, Aug. 2007.

[34] Y. J. Sung, "Circularly polarized square patch antenna with asymmetrical Y-shaped feed structure," Electron. Lett., vol. 46, no. 19, pp. 1309–1310, Sep. 2010.

[35] K. L. Chung and A. S. Mohan, "A systematic design method to obtain broadband characteristics for singly-fed electromagnetically coupled patch antennas for circular polarization," IEEE Trans. Antennas Propag., vol. 51, no. 12, pp. 3239–3248, Dec. 2003.

[36] M. S. Hossain, S. I. Latif, S. K. Sharma, and M. S. Alam, "Hybrid perturbations in stacked ring-patch antennas for wide beamwidth circular polarization," in Proc. Int. Symp. IEEE Antennas Propag., 2016, pp. 27– 28.

[37] Z. H. Jiang and D. H.Werner, "A compact, wideband circularly polarized co-designed filtering antenna and its application for wearable devices with low SAR," IEEE Trans. Antennas Propag., vol. 63, no. 9, pp. 3808–3818, Sep. 2015.

[38] Q.-S. Wu, X. Zhang, and L. Zhu, "A wideband circularly polarized patch antenna with enhanced axial ratio bandwidth via co-design of feeding network," IEEE Trans. Antennas Propag., vol. 66, no. 10, pp. 4996–5003, Oct. 2018.

[39] B. J. Xiang, S. Y. Zheng, Y. M. Pan, and Y. X. Li, "Wideband circularly polarized dielectric resonator antenna with bandpass filtering and wide harmonics suppression response," IEEE Trans. Antenna Propag., vol. 65, no. 4, pp. 2096–2101, Apr. 2017.

[40] X. M. Qing, "Broadband aperture-coupled circularly polarized microstrip antenna fed by a three-stub hybrid coupler," Microw. Opt. Technol. Lett., vol. 40, no. 1, pp. 38–41, Jan. 2004.

[41] K.-L. Wong and T.-W. Chiou, "Broad-band single-patch circularly polarized microstrip antenna with dual capacitively coupled feeds," IEEE Trans. Antennas Propag., vol. 49, no. 1, pp. 41–44, Jan. 2001.

[42] M. He, X. Ye, P. Zhou, G. Zhao, C. Zhang, and H. Sun, "A small-size dualfeed broadband circularly polarized U-slot patch antenna," IEEE Antennas Wireless Propag. Lett., vol. 14, pp. 898–901, 2015.

[43] J. Zhuang, Y. Zhang, W. Hong, and Z. Hao, "A broadband circularly polarized patch antenna with improved axial ratio," IEEE Antennas Wireless Propag. Lett., vol. 14, pp. 1180–1183, 2015.

[44] C.-X. Mao, S. Gao, Y. Wang, Q.-X. Chu, and X.-X. Yang, "Dual-band circularly polarized shared-aperture array for C-/X-band satellite communications," IEEE Trans. Antennas Propag., vol. 65, no. 10, pp. 5171–5178, Oct. 2017.

[45] C.-X.Mao, S. Gao, Y.Wang, and J. T. S. Sumantyo, "Compact broadband dual-sense circularly-polarized microstrip antenna/array with enhanced isolation," IEEE Trans. Antennas Propag., vol. 65, no. 12, pp. 7073–7082, Dec. 2017.

[46] Q.-S. Wu, X. Zhang, and L. Zhu, "Co-design of a wideband circularly polarized filtering patch antenna with three minima in axial ratio response," IEEE Trans. Antennas Propag., vol. 66, no. 10, pp. 5022–5030, Oct. 2018.